Kovove Mater. 56 2018 379–387
DOI: 10.4149/km_2018_6_379

The tribocorrosion behavior of Ni-P and Ni-P-ZrO_2 coatings

F. Tabatabaei[1]*, S. Vardak[2], S. Alirezaei[1], K. Raeissi[2]

[1]*Department of Materials Engineering, Naghshejahan Institute of Higher Education, 81435-118, Baharestan, Isfahan, Iran*
[2]*Department of Materials Engineering, Isfahan University of Technology, Isfahan 84156-83111, Iran*

Received 15 May 2018, received in revised form 5 July 2018, accepted 27 July 2018

Abstract

In this research, tribocorrosion behavior of Ni-P-ZrO_2 electroless composite coating has been investigated in 3.5 wt.% NaCl solution. The steel samples were deposited by electroless deposition to form Ni-P and Ni-P-ZrO_2 coatings. XRD and SEM were used to evaluate the microstructure of the coatings. Also, the corrosion and tribocorrosion behavior of the coatings have been investigated in 5 wt.% NaCl electrolytes. The results showed that the repassivation rate of Ni-P-ZrO_2 composite coating was higher than the mechanical depassivation rate. Also, the corrosion resistance of the Ni-P coating was lower than that of Ni-P-ZrO_2 composite coating after tribocorrosion. Moreover, the synergistic effects of corrosion and wear at an anodic potential (–100 $mV_{Ag/AgCl}$) indicated that corrosion had more contribution to the weight loss in Ni-P coating rather than that of Ni-P-ZrO_2 coating.

K e y w o r d s: tribocorrosion, electroless, composite, zirconia, coating

1. Introduction

Tribocorosion is a complex process of chemical, electrochemical and mechanical degradation of the materials during sliding, rolling or erosion conditions in a corrosive environment [1–3]. The mechanism of tribocorrosion is not yet fully understood [1]. Tribocorrosion has been observed in different applications such as automotive, aerospace, chemical, microelectronics, mining, and marine industries [4, 5]. Electroless Ni-P coating is one of the suitable choices for tribocorrosion purposes especially in the saline environment, because of its excellent corrosion and wear resistance, low friction, and uniform thickness. Furthermore, it has been reported that the co-deposition of metallic or non-metallic particles within the Ni-P matrix could change the mechanical, tribological and corrosion behaviors of the deposits [6–14]. The corrosion resistance of the composite coatings can be strongly influenced by several factors such as particle size, particle content and uniform distribution of the particles. The particles can reduce the effective surface area of the metallic matrix after exposure to the corrosive electrolyte. They can also fill the micro holes and submicron defects produced during electroless deposition [15]. The improvement of the corrosion resistance in saline solution has been extensively reported in different types of composite coatings such as NiP-CeO_2, NiP-TiO_2, NiP-Si_3N_4, NiP--PVC, NiP-nanoSiO_2, NiP-CNT, NiP-ZrO_2, NiP-nano SiC, and NiP-ZrO_2-Cu [6–14]. The synergistic effects of corrosion and wear in NaCl aqueous solution have been studied by several investigations [16–18]. Lee and co-workers showed that the corrosion film containing PO_4^{-3} ions has improved the lubrication property on the sliding surface of electrodeposited NiP coatings [17, 18]. Malfatti et al. have also evaluated the tribocorrosion behavior of heat-treated NiP and NiP-SiC coatings obtained by an electrodeposition process. It was found that a higher amount of SiC particles increases the wear resistance and decreases the corrosion resistance of the composite coatings [9]. Zirconia as a remarkable ceramic material has been widely used in oxygen pumps and sensors, fuel cells and thermal barrier coatings [11]. Composite coatings containing ZrO_2 particles could demonstrate the suitable mechanical and tribological behaviors [12, 13, 19, 20]. Szczygieł et al. reported the improvement of wear resistance

*Corresponding author: e-mail address: ftt_aim@yahoo.com

Table 1. The characteristics of electroless baths

Coating	CTAB ($mg\,L^{-1}$)	ZrO_2 ($g\,L^{-1}$)
Ni-P	0	0
Ni-P-ZrO_2	10	5

of electroless alloy coatings by co-deposition of ZrO_2 particles within Ni-P coatings [13]. Because of the significant characteristics of zirconia reinforcement and the great properties of Ni-P matrix especially in oil and petroleum applications, the corrosion and tribocorrosion behaviors of Ni-P-ZrO_2 coatings have been investigated in the present research.

2. Experiment

2.1. Coating process

Electroless nickel coating was deposited on a disc shape carbon steel (AISI 1045) substrate with 20 mm in diameter and 5 mm in thickness. The specimens were mechanically ground by using 80–1200 grit silicon carbide papers and then they were degreased in $10\,g\,L^{-1}$ sodium hydroxide solution at 80 ± 2 ℃ for 10 min. A commercial electroless nickel bath (Schlotter-SLOTONIP 70A) was used containing $7\,g\,L^{-1}$ nickel and $30\,g\,L^{-1}$ NaH_2PO_2. The deposition temperature was 90 ± 2 ℃, and pH was adjusted on 4.7 ± 0.1. The deposition time was 3 h, and the stirring rate of 250 rpm was employed to prevent the sedimentation of ZrO_2 particles in the plating bath. The electroless composite bath contained $5\,g\,L^{-1}$ monoclinic ZrO_2 powder (with the average particle size of 5 μm, Sigma Aldrich). Two types of coatings were deposited on the steel substrates according to Table 1. The solution used for electroless plating was commercial, and it consisted of a suitable amount of the stabilizer, so there was no requirement to use CTAB.

2.2. Coating characterization

X-ray diffractometer (XRD, Philips X'pert) with Cu K_α radiation was used to analyze the structure of the coatings. The volumetric percentage (vol.%) of ZrO_2 particles in the metallic matrix was estimated by image analysis of the cross-section micrographs. Surface morphology, particle distribution, and the wear tracks were evaluated by a scanning electron microscope (SEM, Philips XL30). The chemical composition of the coatings was also determined by energy dispersive spectroscopy (EDS) analysis. The volume loss of the coatings in the wear tracks was measured by utilizing a 2D profilometer (Mitutoyo Surftest-SJ210)

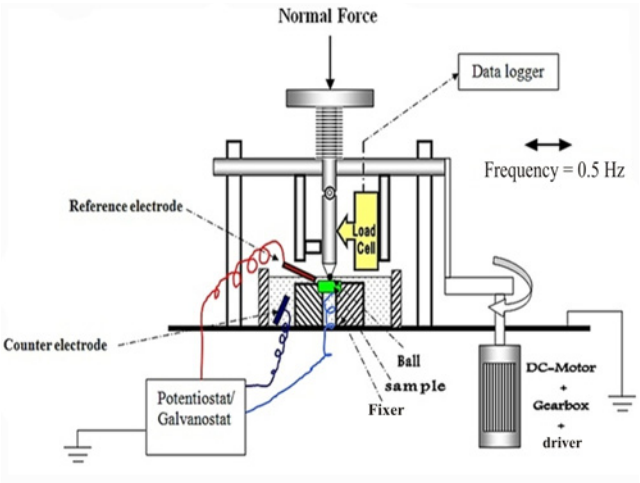

Fig. 1. Scheme of tribocorrosion apparatus.

after anodic (–100 $mV_{Ag/AgCl}$) and cathodic (–500 $mV_{Ag/AgCl}$) tribocorrosion experiments. The weight loss of the coatings was also calculated according to the densities of the Ni-P matrix and ZrO_2 particles and also the content of the zirconia in the composite coating.

2.3. Electrochemical measurement

Tribocorrosion experiments were performed at room temperature in 3.5 wt.% NaCl solution with pH 6.7 ± 0.1 by using a reciprocating ball-on-plate tribometer (Fig. 1). The tribocorrosion system was connected to EG&G Potentiostat/Galvanostat (model 263A) with a three-electrode cell consisting of Ag/AgCl reference electrode, Pt counter electrode and coating sample as the working electrode. To assess the influence of ZrO_2 particles on the corrosion resistance of Ni-P coating, cyclic polarization technique was used in 3.5 wt.% NaCl solution. The corrosion behavior of the coatings was also evaluated by electrochemical impedance spectroscopy (EIS) before and after the tribocorrosion experiments. EIS measurements were conducted by applying a sinusoidal potential oscillation (amplitude ± 5 mV) with the frequency range of 100 kHz to 10 MHz. The wear test was performed under a 10 N applied load by a SiC ball with a diameter of 7 mm. The stroke length was 10 mm, and the number of sliding cycles was 1800 at 0.5 Hz. The electrochemical measurements started after reaching OCP to the constant value.

3. Results and discussion

3.1. Microstructure and surface morphology

Figure 2 demonstrates XRD patterns of zirconia

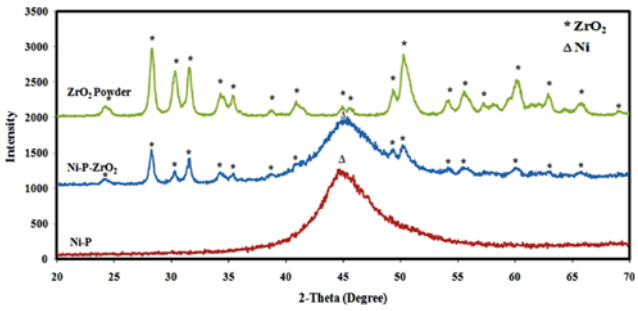

Fig. 2. XRD patterns of ZrO_2 powder, Ni-P and Ni-P--ZrO_2.

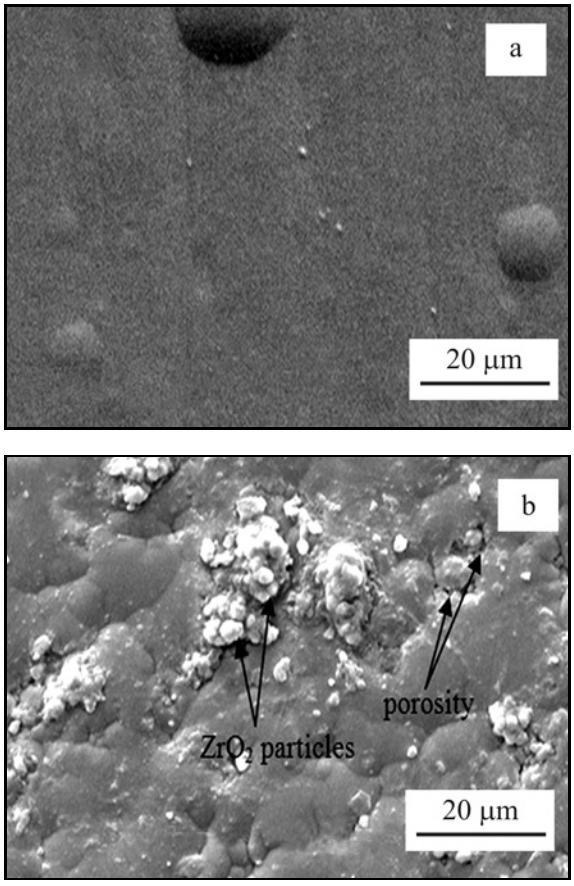

Fig. 3. SEM micrographs of (a) Ni-P and (b) Ni-P-ZrO_2 coatings.

powder, Ni-P coating, and Ni-P-ZrO_2 composite coating. XRD analysis clearly shows a broad peak in the pattern of Ni-P coating indicating a completely amorphous structure. The Ni-P-ZrO_2 composite coating also consists of an amorphous Ni-P matrix and a crystalline structure of zirconia. Also, EDX analysis reveals a high phosphorous content (10–11 wt.% P) in both types of the coatings according to Table 2. Keong and co-workers have reported an amor-

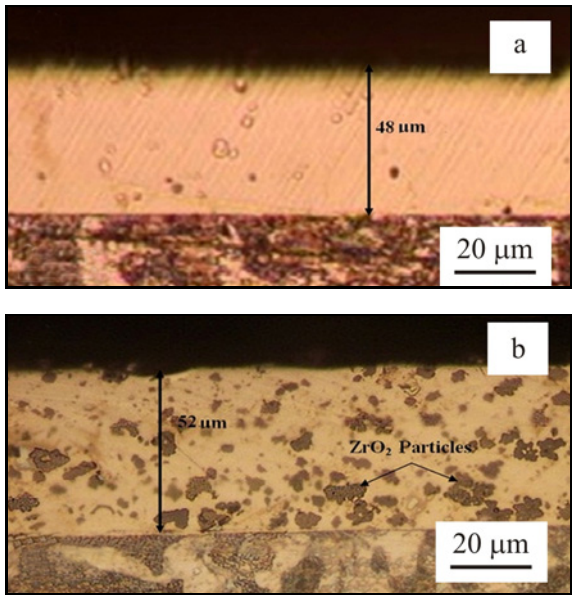

Fig. 4. Optical cross-section micrographs of the coatings; (a) Ni-P and (b) Ni-P-ZrO_2.

Table 2. EDX analysis of Ni-P and Ni-P-ZrO_2 coatings

Coating	Phosphorus content (wt.%)
Ni-P	10.5
Ni-P-ZrO_2	10

phous structure in high phosphorus Ni-P electroless coatings at the 2θ position of 35–55° [21]. Figure 3 shows the SEM micrographs of as-plated Ni-P and Ni-P-ZrO_2 composite coating, respectively. The surface morphology of the Ni-P coating in Fig. 3a indicates a nearly smooth surface morphology. Figure 3b also demonstrates the embedment of zirconia particles within the Ni-P matrix. As illustrated in Fig. 4b, ZrO_2 particles were entrapped in Ni-P metallic matrix but with a few agglomerations. It seems that the amount of the surfactant was not enough to disperse the particles uniformly. The volumetric percent of ZrO_2 particles in Ni-P-ZrO_2 coating was determined about 26 % (Table 3). The cationic surfactant was used in minor amounts for the composite plating whereas the particles should achieve a positive zeta potential to attract toward the substrate as well as the modification of surface wetting of particles. Suitable amounts of CTAB can also prevent the agglomeration between the particles and unwanted deposition of nickel on the particles. The suspended particles in the electroless solution can easily move to the surface of the substrate by mechanical agitation and then, they can co-deposit within Ni-P matrix to form a composite coating. The embedment of the particles into the matrix can be related

Table 3. The characteristics of Ni-P and Ni-P-ZrO_2 coatings

Coating	ZrO_2 content (vol.%)	Thickness (μm)
Ni-P	0	48
Ni-P-ZrO_2	26	52

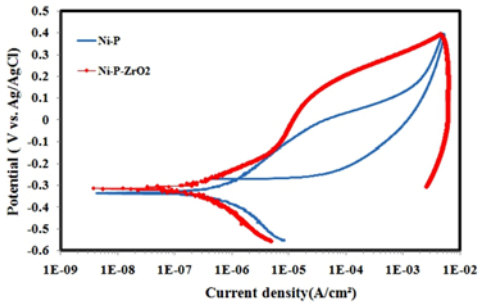

Fig. 5. Cyclic polarization curves of Ni-P and Ni-P-ZrO_2 coatings in 3.5 wt.% NaCl solution.

to the physical and chemical adsorption between the reinforcements and Ni-P coating [22, 23]. A few porosities can also be found in Ni-P-ZrO_2 composite coating because of the high production of hydrogen during the growth of Ni-P coating and the embedment of the particles into the metallic matrix [24]. Figure 4 shows the cross-section micrograph of the coatings. Although the plating time was the same for Ni-P and Ni-P-ZrO_2 coatings (3 h), the thickness of the composite deposit was achieved higher than that of free-particle deposit. The existence of the particles in the Ni-P matrix and also the high growth rate of Ni-P matrix may increase the thickness of Ni-P-ZrO_2 coating.

3.2. Cyclic polarization

As shown in Fig. 5, the corrosion potential (E_{corr}) changed slightly to the higher negative values in the Ni-P-ZrO_2 coating, and the corrosion current density (i_{corr}) was increased by incorporation of ZrO_2 particles into Ni-P coating. The existence of hysteresis loops in cyclic polarization curves implies the pitting corrosion. The parameters such as E_{corr}, i_{corr}, pitting potential (E_{pit}) and repassivation potential (E_{rp}) are indicated in Table 4. It seems that the co-deposition

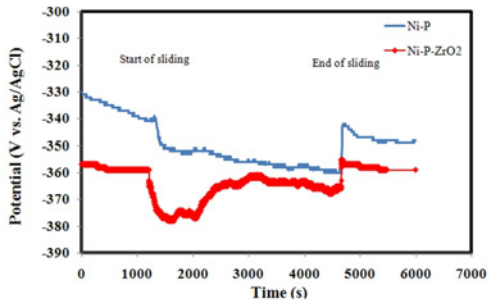

Fig. 6. The variation of OCP versus time for Ni-P and Ni-P-ZrO_2 coatings during tribocorrosion.

of ZrO_2 particles can decrease E_{pit}. The higher difference between E_{pit} and E_{rp} in Ni-P coating implies the lower repassivation capability of the passive layer and the more tendency to pitting corrosion [25]. Because of the lower E_{pit} and $E_{pit} - E_{corr}$ in the composite coating, the susceptibility of Ni-P-ZrO_2 to pitting corrosion is more than that of Ni-P coating. Despite the existence of inert ceramic ZrO_2 particles in Ni-P matrix, the formation of the porosities during electroless deposition can be the main reason of lower resistance to pitting corrosion [15]. The ceramic reinforcements can also act as the barrier regions to the further propagation of pits into Ni-P matrix.

3.3. Tribocorrosion at open circuit potential

The variation of Open Circuit Potential (OCP) before sliding was small for all the coatings indicating the stable passive conditions as shown in Fig. 6. A drop of OCPs to the cathodic values can also be shown at the onset of sliding. At the first stroke of SiC ball, the protective layer is removed, and the surface becomes active in worn track [2, 5]. So, it can create a galvanic cell between the passive surface area and the bare coating to cause a drastic decrease in the corrosion potential [3, 5]. By further sliding, potential shifts to the higher values in the composite coating but it changed slightly to the lower values in Ni-P coating. In the worn area, there is a competition between mechanical depassivation and electrochemical passivation [2]. When the mechanical depassivation removes the protective layer, the worn track surface is exposed to the severe corrosion. Then, the passive film is recovered again, and it causes a gradual positive shift of

Table 4. Corrosion parameters of Ni-P and Ni-P-ZrO_2 coatings in 3.5 wt.% NaCl solution

Coating	OCP (mV)	E_{corr} (mV)	i_{corr} (μA/cm^2)	E_{pit} (mV vs. Ag/AgCl)	E_{rp} (mV vs. Ag/AgCl)	$E_{pit} - E_{rp}$ (mV vs. Ag/AgCl)	$E_{pit} - E_{corr}$ (mV vs. Ag/AgCl)
Ni-P	–312	–300	0.28	30	< –312	> 342	330
Ni-P-ZrO_2	–330	–325	0.6	–50	–280	230	275

the corrosion potential [2]. The equilibrium between the mechanical damage and the electrochemical repassivation at the metal surface requires enough time as shown in Fig. 6. In tribocorrosion, galvanic corrosion can occur theoretically: (1) galvanic coupling between the completely depassivated wear track and its surrounded region, or (2) short-range galvanic coupling between depassivated or passive area in the wear track and the region around it [26]. Equation (1) expresses the galvanic cell model for tribocorrosion at OCP [26, 27]:

$$E_c = E_{corr} + a_c - b_c \log i_a - b_c \log(A_a/A_c), \qquad (1)$$

where E_c is the measured OCP during sliding without any physical separation between the anode and cathode; a_c and b_c are the constants calculated from Tafel equations; i_a is the anodic current density produced during the depassivation process inside the wear track; and A_a and A_c are the surface areas of the anode and the cathode, respectively [27]. According to Eq. (1), cathode potential value (E_c) in the galvanic coupling depends on two factors: the anodic current (i_a) and the anode-to-cathode area ratio (A_a/A_c) [2, 5, 27]. The anodic current is related to the cyclic depassivation/repassivation process in the worn area. It normally attains a steady value during the tribocorrosion of a passive metal [28]. The OCP variations of Ni-P-ZrO_2 (Fig. 6) also show a greater repassivation rate in worn surfaces of the composite coating compared to the mechanical depassivation. After sliding, E_c changes to the positive values with the small fluctuations. Hassani et al. have correlated the OCP variations to the competition between the mechanical depassivation and electrochemical repassivation [2]. After termination of the wear test (i.e., after 1800 cycles), the wear scar has enough time to repassivate. It can be observed in Fig. 6 that OCPs reach their initial values as the result of repassivation.

3.4. Worn surfaces

Figure 7 shows the micrographs of worn tracks after tribocorrosion tests at OCP value. It represents the parallel scratches in the sliding direction of the Ni-P coating caused by a severe abrasive wear mechanism (Fig. 7a). The worn surface of Ni-P-ZrO_2 composite coating demonstrates that ZrO_2 particles have been detached from the coating during the wear process (Fig. 7b). The tribological and mechanical behaviors of hard particle-reinforced composites strongly depend on the interfacial bonding between the matrix and the reinforcements [29, 30]. As mentioned in Fig. 3b, the formation of the voids in the interface of ZrO_2 particles and Ni-P matrix causes the subsequent cracking and the detachment of ZrO_2 particles from the coating during sliding [28].

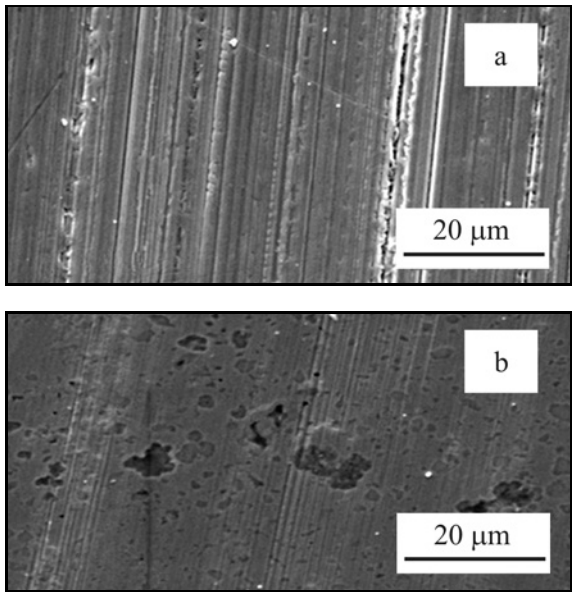

Fig. 7. SEM micrographs of wear track in (a) Ni-P and (b) Ni-P-ZrO_2 coatings.

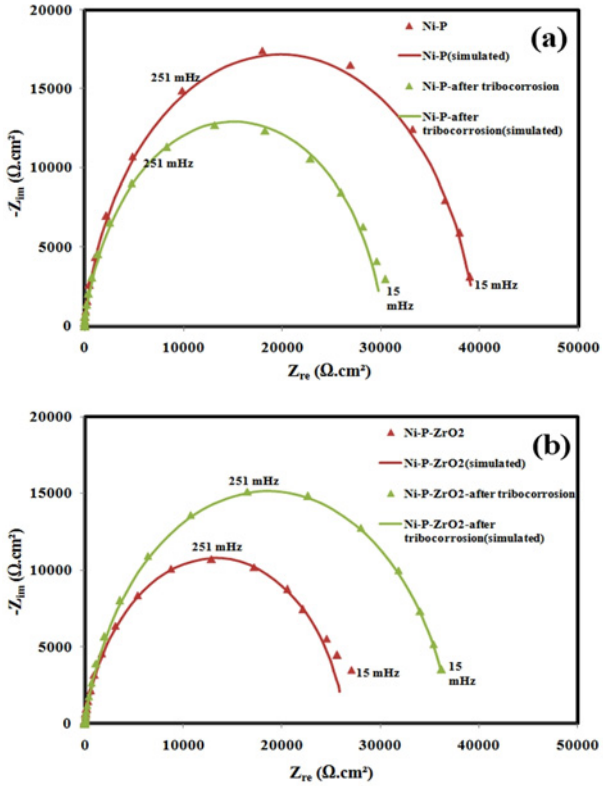

Fig. 8. Nyquist and Bode plot of the coatings before and after the tribocorrosion test.

3.5. EIS studies

Figure 8 shows the Nyquist plots representing the EIS (Electrochemical Impedance Spectroscopy) spec-

Table 5. The EIS data of Ni-P and Ni-P-ZrO_2 coatings in 3.5 wt.% NaCl solution

Coating	R_s ($\Omega\,cm^2$)	R_{ct} ($k\Omega\,cm^2$)	C_{dl} (Y_0 ($\mu F\,cm^2$))	n
Ni-P	0.5	39.6	44.7	0.90
Ni-P (after tribocorrosion)	0.5	30.1	78.2	0.90
Ni-P-ZrO_2	2.4	26.4	80.0	0.87
Ni-P-ZrO_2 (after tribocorrosion)	2.7	37.2	62.3	0.87

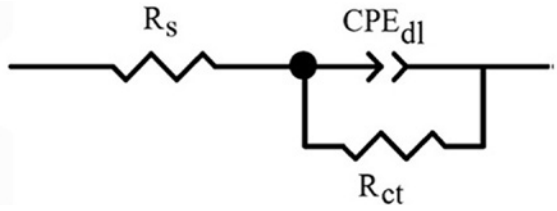

Fig. 9. Equivalent electrical circuit model.

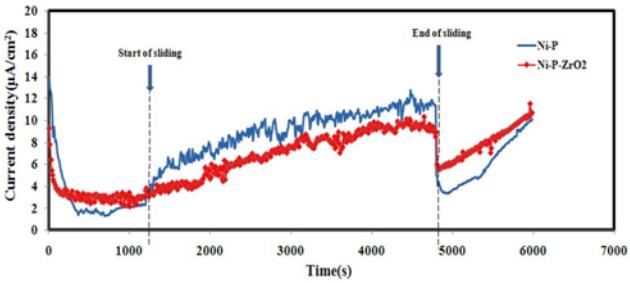

Fig. 10. Current density variations of the coatings under –100 $mV_{Ag/AgCl}$ polarization during tribocorrosion.

tra of the coatings at OCP values before and after the tribocorrosion test. Nyquist plots demonstrate the capacitive semicircles with different diameters. It seems that there is only a time constant as the result of the uniform corrosion in the coating/electrolyte interface [10, 12]. So, the corrosive electrolyte cannot penetrate into the defects of Ni-P and Ni-P-ZrO_2 composite coatings. This behavior has also been observed in NiP-CeO_2, NiP-TiO_2, NiP-Si_3N_4, NiP-nano SiO_2 and Ni-P-CNT coatings [6, 31]. The equivalent electrical circuit model in Fig. 9 describes the corrosion behavior of the coatings. The equivalent circuit specifies a charge transfer resistance (R_{ct}) parallel to the double layer capacitance (C_{dl}) that it can be replaced with a constant phase element (CPE). The impedance of CPE is expressed by the following equation [32]:

$$Z_Q = [Y_0(j\omega)^n]^{-1}, \quad (2)$$

where Z_Q is CPE impedance ($\Omega\,cm^2$), Y_0 is CPE admittance ($\mu F\,cm^{-2}$), and ω is the angular frequency ($rad\,s^{-1}$). The parameter n is a constant value showing the degree of deviation from the ideal capacitive behavior. Table 5 represents EIS data obtained by Nyquist plots and the equivalent circuit. Figure 8a demonstrates a decrease in the Nyquist plot diameter of Ni-P coating after the tribocorrosion test at OCP value. The value of R_{ct} decreases when the number/size of pinholes increases. It can cause the deterioration of the passive layer especially in the worn area [12, 33]. According to Table 5, the embedment of ZrO_2 particles in Ni-P matrix can decrease the charge transfer resistance (R_{ct}) and then it can increase the double layer capacitance (C_{dl}). These observations are in agreement with the results achieved by Stankiewicz in Ni-P-14 wt.%ZrO_2 composite coating [12]. The EIS data show that the charge transfer resistance of Ni-P-ZrO_2 composite coating (R_{ct}) has been increased from 26.4 to 37.2 K $\Omega\,cm^2$ after tribocorrosion. It is comparable to the R_{ct} values of Ni-P coating before and after tribocorrosion. While ZrO_2 particles are detached from the surface of the coating during sliding, new active regions can be created. So, the repassivation rate of the new area is higher in the lack of the ZrO_2 particles in the composite coating. Thus, the charge transfer resistance (R_{ct}) of worn track area is increased after the end of the tribocorrosion test.

3.6. Potentiostatic tribocorrosion

The variation of current density versus time at –100 $mV_{Ag/AgCl}$ has been shown in Fig. 10. By the formation of the passive layer, the current density is decreased, and it becomes nearly stable. It has been reported that a multilayer passive film including nickel phosphate layer and phosphorus-rich layer develops on the surface of the Ni-P coating by applying anodic overpotential [17]. As shown in Fig. 10, there is a significant rise in anodic current at the start of the sliding for both types of the coatings because of a high degree of anodic dissolution. During the sliding process, the current density is increased and subsequently, it returns to the value before the start of sliding. Since the detachment of the particles improves the repassivation rate of the composite coatings, the current density of the composite coating is lower than that of the free-particle coating during sliding [9].

3.7. Estimation of the weight loss

According to ASTM G119-09, the synergistic ef-

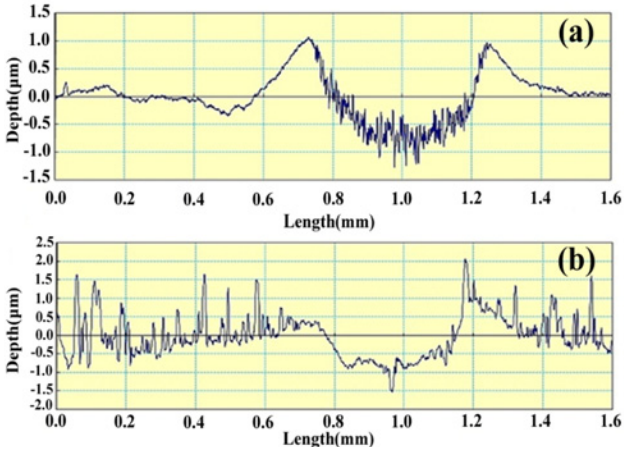

Fig. 11. Roughness profiles of the coatings after anodic tribocorrosion; (a) Ni-P and (b) Ni-P-ZrO_2.

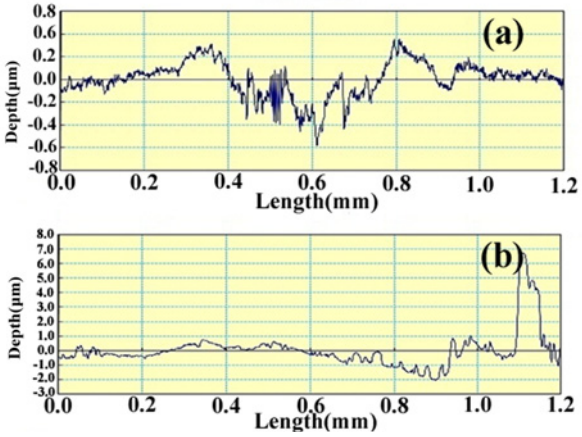

Fig. 12. Roughness profile after cathodic tribocorrosion; (a) Ni-P and (b) Ni-P-ZrO_2.

fects of wear and corrosion on the weight loss of the coatings in tribocorrosion (W_{total}) can be expressed as follows [18, 34]:

$$W_{\text{total}} = W_{\text{wear}} + W_{\text{corr}} + \Delta W. \tag{3}$$

In Eq. (3), W_{total} is the total weight loss in anodic tribocorrosion, W_{wear} is the summation of the weight loss related to the pure wear (W_{wear}) calculated from cathodic potentiostatic tribocorrosion, W_{corr} is the weight loss due to the pure corrosion and ΔW is the synergistic effect of corrosion and wear. ΔW can be further divided into two parts as follows [18, 34]:

$$\Delta W = \Delta W_{\text{corr}} + \Delta W_{\text{wear}}, \tag{4}$$

where ΔW_{corr} denotes the wear-enhanced corrosion and ΔW_{wear} explains the corrosion-enhanced wear. The current density in the wear track (Δi_{corr}) can be determined by subtracting the average current measured before sliding (i_{pure}) from the average current measured during sliding (i_{corr}). By using this differential value, ΔW_{corr} can be calculated by Faraday's law (Eq. (5)) [2, 18]:

$$\Delta W_{\text{corr}} = (M/nF)\Delta i_{\text{corr}} St, \tag{5}$$

where M is the molar mass of metallic matrix, Δi_{corr} ($\mu\text{A cm}^{-2}$) is the current density in the wear track, S is the surface area of the coating (cm^2), t is the test duration (s), n is number of electrons involved in the electrochemical reaction and F is the Faraday constant (96487 C mol^{-1}). The synergistic effect of corrosion on wear can then be calculated accordingly:

$$\Delta W_{\text{wear}} = W_{\text{total}} - W_{\text{wear}} - W_{\text{corr}} - \Delta W_{\text{corr}}. \tag{6}$$

In the method mentioned above, the calculation of mass loss in the worn track is only possible, and the term of W_{corr} can be omitted. On the other hand, W_{corr} belongs to the corrosion on the whole surface. Figures 11 and 12 show the roughness profiles of worn tracks in Ni-P and Ni-P-ZrO_2 coatings obtained from the potentiostatic tribocorrosion test at –100 and –500 $\text{mV}_{\text{Ag/AgCl}}$. The synergistic effects of wear and corrosion can be calculated using Eqs. (5) and (6). Table 6 shows that the contribution of wear-enhanced corrosion (ΔW_{corr}) is more than that of the other factors in the synergistic weight loss of Ni-P coating. This behavior has been mentioned by Dearnley et al. as Type I corrosion–wear mechanism [35]. On the other hand, the synergistic weight loss of Ni-P-ZrO_2 coating has been more influenced by the weight loss of corrosion-enhanced wear (ΔW_{wear}). According to Fig. 10(a), Δi_{corr} ($i_{\text{corr}} - i_{\text{pure}}$) of Ni-P is higher than that of Ni-P-ZrO_2. So, the pitting rate is higher, and the passive film cannot be regenerated. It can be deduced that the synergistic effect of wear on corrosion (ΔW_{corr}) in Ni-P is remarkable. Also, Table 6 represents that ΔW_{wear} of Ni-P-ZrO_2 is about 2 times of W_{wear} due to the synergistic effect of corrosion on wear. While corrosion at anodic potential facilitates the detachment of ZrO_2 particles from matrix/particle interfaces, the synergistic effect of corrosion on wear is more than that of wear on corrosion. Lee et al. explained that the wear could remove the corrosion product from the surface and it could severely reduce the corrosion resistance [18].

4. Conclusions

1. The variation of the OCPs in tribocorrosion experiments showed that the repassivation rate is higher than mechanical depassivation in Ni-P-ZrO_2 composite coating. While ZrO_2 particles were detached from

Table 6. The weight loss of the coatings calculated from potentiostatic tribocorrosion

Coating	$\Delta W_{wear}/\Delta W$ (%)	$\Delta W_{corr}/\Delta W$ (%)	ΔW_{wear} (μg)	ΔW_{corr} (μg)	W_{wear} (μg)	W_{total} (μg)
Ni-P	31	69	4 ± 0.5	9 ± 0.5	14 ± 0.5	27 ± 0.5
Ni-P-ZrO_2	76	24	22 ± 0.5	7 ± 0.5	8 ± 0.5	37 ± 0.5

the surface of composite coatings, new active metallic surfaces were created during sliding. It could cause severe corrosion in the worn track by type I corrosion–wear mechanism and also a gradual positive shift in potential.

2. Ni-P-ZrO_2 coating showed the lower current density than that of Ni-P coating during sliding. Also, enhancement of R_{ct} in the composite coating confirmed the formation of the passive protective layers during sliding.

3. Although, the synergistic weight loss in Ni-P-ZrO_2 coating was influenced by the corrosion effect on wear, the weight loss of Ni-P coating at anodic potential was due to the effect of wear on corrosion. Also, the corrosion resistance of Ni-P-ZrO_2 coating was higher than its wear resistance during tribocorrosion experiments.

Acknowledgement

The authors would like to thank N. Arabian for his assistance in the experimental works.

References

[1] Benea, L., Wenger, F., Ponthiaux, P., Celis, J. P.: Wear, *266*, 2009, p. 398. doi:10.1016/j.wear.2008.04.018
[2] Hassani, S., Raeissi, K., Azzi, M., Li, D., Golozar, M. A., Szpunar, J. A.: Corr. Sci., *51*, 2009, p. 2371. doi:10.1016/j.corsci.2009.06.026
[3] Ponthiaux, P., Wenger, F., Drees, D., Celis, J. P.: Wear, *256*, 2004, p. 459. doi:10.1016/S0043-1648(03)00556-8
[4] Bratu, F., Benea, L., Celis, J. P.: Surf. Coat. Technol., *201*, 2007, p. 6940. doi:10.1016/j.surfcoat.2006.12.027
[5] Tabatabaei, F., Raeissi, K., Saatchi, A., Kazmanli, K., Ürgen, M.: Surf. Eng., *29*, 2013, p. 671. doi:10.1179/1743294413Y.0000000175
[6] Alishahi, M., Monirvaghefi, S. M., Saatchi, A., Hosseini, S. M.: Appl. Surf. Sci., *258*, 2012, p. 2439. doi:10.1016/j.apsusc.2011.10.067
[7] Allahkaram, S. R., Honarvar-Nazari, M., Mamaghani, S., Zarebidaki, A.: Mater. Des., *32*, 2011, p. 750. doi:10.1016/j.matdes.2010.07.030
[8] Balaraju, J. N., Sankara-Narayanan, T. S. N., Seshadri, S. K.: J. Appl. Electrochem., *3*, 2003, p. 807. doi:10.1023/A:1025572410205
[9] Malfatti, C. F., Veit, H. M., Santos, C. B., Metzner, M., Hololeczek, H., Bonino, J. P.: Tribol. Lett., *36*, 2009, p. 165. doi:10.1007/s11249-009-9471-1
[10] Rabizadeh, T., Allahkaram, S. R.: Mater. Des., *32*, 2011, p. 133. doi:10.1016/j.matdes.2010.06.021
[11] Ranganatha, S., Venkatesha, T. V., Vathsala, K.: Mater. Res. Bullet., *47*, 2012, p. 635. doi:10.1016/j.materresbull.2011.12.024
[12] Stankiewicz, A., Masalski, J., Szczygieł, B.: Mat. Corr., *64*, 2013, p. 908. doi:10.1002/maco.201206856
[13] Szczygieł, B., Turkiewicz, A., Serafińczuk, J.: Surf. Coat. Technol., *202*, 2008, p. 1904. doi:10.1016/j.surfcoat.2007.08.016
[14] Edwin Sahayaraj, M., Winowlin Jappes, J. T., Siva, I., Rajini, N.: Sci. Eng. Compos. Mater., *23*, 2016, p. 309. doi:10.1515/secm-2014-0134
[15] Bakhit, B., Akbari, A.: Surf. Coat. Technol., *206*, 2012, p. 4964. doi:10.1016/j.surfcoat.2012.05.122
[16] Bailey, R., Sun, Y.: J. Mater. Eng. Perform., *24*, 2015, p. 1669. doi:10.1007/s11665-015-1441-1
[17] Lee, H. B., Wuu, D. S., Lee, C. Y., Lin, C. S.: Tribol. Int., *43*, 2010, p. 235. doi:10.1016/j.triboint.2009.05.031
[18] Lee, H. B., Wuu, D. S., Lee, C. Y., Lin, C. S.: Tribol. Int., *44*, 2011, p. 1603. doi:10.1016/j.triboint.2011.04.011
[19] Gao, J., Sun, W. C., Shi, Q., Wang, Y., Tian, M. M.: Mater. Sci. Forum, *817*, 2015, p. 449. doi:10.4028/www.scientific.net/MSF.817.449
[20] Yang, Y., Chen, W., Zhou, C., Xu, H., Gao, W.: Appl. Nanosci., *1*, 2011, p. 19. doi:10.1007/s13204-011-0003-6
[21] Keong, K. G., Sha, W., Malinov, S.: J. Mat. Sci., *37*, 2002, p. 4445. doi:10.1023/A:1020641611389
[22] Malfatti, C. F., Ferreira, J. Z., Oliveira, C. T., Rieder, E. S., Bonino, J. P.: Mat. Corr., *63*, 2012, p. 36. doi:10.1002/maco.200905611
[23] Zhang, X., Qin, J., Das, M. K., Hao, R., Zhong, H., Thueploy, A., Limpanart, S., Boonyongmaneerat, Y., Ma, M., Liu, R.: Sci. Rep., *6*, 2016, p. 1. doi:10.1038/srep22285
[24] Li, C., Wang, Y., Pan, Z.: Mater. Des., *47*, 2013, p. 443. doi:10.1016/j.matdes.2012.12.021
[25] Pardo, A., Merino, M. C., Coy, A. E., Viejo, F., Arrabal, R., Matykina, E.: Corr. Sci., *50*, 2008, p. 1796. doi:10.1016/j.corsci.2008.04.005
[26] Papageorgiou, N., Mischler, S.: Tribol. Lett., *48*, 2012, p. 271. doi:10.1007/s11249-012-0022-9
[27] Espallargas, N., Johnsen, R., Torres, C., Muñoz, A. I.: Wear, *307*, 2013, p. 190. doi:10.1016/j.wear.2013.08.026
[28] Sawla, S., Das, S.: Wear, *257*, 2004, p. 555. doi:10.1016/j.wear.2004.02.001
[29] Byengsoo, L., Chul-ju, K., Bumjoon, K., Untae, S., Seyoung, O., Byung-ho, S., Jee-hoon, C., Seunghyun, B.: Nanotechnol., *17*, 2006, p. 5759. doi:10.1088/0957-4484/17/23/008

[30] Zakaulla, M., Anwar-Khan, A. R., Mukunda, P. G.: Int. J. Emerging Sci. Eng., *2*, 2014, p. 8. https://www.ijese.org/download/volume-2-issue-5/
[31] Balaraju, J., Sankara Narayanan, T., Seshadri, S.: J. Solid State Electrochem., *5*, 2001, p. 334. doi:10.1007/s100080000159
[32] Marcus, P., Mansfeld, F. B.: Analytical Methods In Corrosion Science and Engineering, Boca Raton, CRC 2005. ISBN: 9780824759520
[33] Azzi, M., Szpunar, J. A.: Biomol. Eng., *24*, 2007, p. 443. doi:10.1016/j.bioeng.2007.07.015
[34] ASTM-G119-09, Standard Guide for Determining Synergism Between Wear and Corrosion, West Conshohocken, ASTM 2016. doi:10.1520/G0119-09R16
[35] Dearnley, P. A., Dahm, K. L., Çimenoglu, H.: Wear, *256*, 2004, p. 469. doi:10.1016/S0043-1648(03)00557-X